Electronic Supplementary Material (ESI) for Chemical Science.

Electronic Supplementary Information

Modulating the Electronic Interactions via Heterostructure Engineering for Energy-Saving Hydrogen Production at High Current Densities

Dongxing Tan*, Xianfang Yin, Jing Wang, Zixuan Zhang, Xiao Zhu, Hengrui Kang and Yuanyuan Feng*

Key Laboratory of Catalytic Conversion and Clean Energy in Universities of Shandong Province, School of Chemistry and Chemical Engineering, Qufu Normal University, Qufu Shandong, 273165, P.R.China.

**Correspondence Email: tandx@qfnu.edu.cn, fengyy@qfnu.edu.cn.*

This PDF file includes:
Experimental Section; Fig. S1 to S15; Table S1.

Experimental

Materials. Nickel nitrate hexahydrate, ammonium molybdate tetrahydrate, N, N-Dimethylformamide (DMF), Potassium hydroxide, absolute ethanol and methanol were provided by Sinopharm Chemical Reagent Beijing Co., Ltd. p-Phthalic acid, tetrafluoroterephthalic acid and nickel foam (NF) were purchased from Aladdin. Pt/C (20 wt% Pt on Vulcan XC-72), RuO_2 and Nafion (5 wt%) were purchased from Sigma-Aldrich. All electrolyte solutions were prepared by using Millipore water (resistivity: ~18.5 MΩ·cm).

Pre-treatment of NF. The NF was ultrasonic treated 3 M hydrochloric acid aqueous solution, deionized water and ethanol for 10 min to remove surface oxides and impurities. Finally, the treated NF was stored in ethanol for later use.

Preparation of electrocatalysts. Preparation of $Ni_{0.2}Mo_{0.8}N$/F,N-C@NF: In a typical synthesis process, appropriate amounts of tetrafluoroterephthalic acid, nickel nitrate hexahydrate and ammonium molybdate tetrahydrate were dispersed into 21 mL of the mixed solution of DMF, ethanol and water (volume ratio= 18:2:1) and stirred at room temperature for 30 min. Next, the solution was transferred into a Teflon liner stainless-steel autoclave, then a piece of NF (2×3 cm^2) was immersed in the mixed solution and the autoclave was sealed and heated at 140 °C for 12 h. After the autoclave cooled to room temperature, the as-prepared sample was washed with ethanol and dried in a vacuum oven at 80 °C for 24 h. The solid was annealed in tube furnace at 500 °C in NH_3 atmosphere for 2 h with a heating rate of 5 °C min^{-1}.

Preparation of $Ni_{0.2}Mo_{0.8}N$/N-C@NF: The preparation process of $Ni_{0.2}Mo_{0.8}N$/N-C@NF is similar to that of $Ni_{0.2}Mo_{0.8}N$/F,N-C@NF, except that tetrafluoroterephthalic acid is replaced by p-Phthalic acid.

Preparation of Ni_3N/F,N-C@NF: The preparation process of Ni_3N/F,N-C@NF is similar to that of $Ni_{0.2}Mo_{0.8}N$/F,N-C@NF, but without ammonium molybdate tetrahydrate.

Preparation of Ni_3N/N-C@NF: The preparation process of Ni_3N/N-C@NF is similar to that of Ni_3N/F,N-C@NF, but without ammonium molybdate tetrahydrate.

Fabrication of Pt/C@NF and RuO_2@NF electrodes: The Pt/C@NF and RuO_2@NF electrodes were prepared by loading samples suspension onto NF. Briefly, the Pt/C, RuO_2 and 10 μL Nafion D-521 dispersion were dispersed in absolute ethanol and ultrasonicated for 1 h to form uniform suspension, and the suspension was loaded on the NF, respectively. The electrode was dried in a vacuum oven at 80 °C for 6 h before electrochemical experiment.

Characterizations. The morphologies of the catalysts were characterized by SEM (HITACHI S-4800). TEM images were taken on JEOL JEM-EM-1011 and JEOL JEM-2100F field-emission high-resolution transmission electron microscope operated at 200 kV. XRD patterns were conducted on a Rigaku D/max 2400 diffractometer with Cu Ka radiation (λ= 0.15418 nm). XPS was carried out with a multipurpose X-ray photoemission spectroscope (Thermo Scientific ESCALAB 250Xi).

A CHI660E electrochemical analyzer (Shanghai Chenhua instrument co. LTD, China) was used in all the electrochemical experiments. All electrochemical experiments were carried out in a three-electrode system. The reference and counter electrodes are Hg/HgO and graphite rod, respectively. All experiments were measured at atmospheric pressure and room temperature. All working electrodes were used for electrochemical experiments with a fixed working area of 0.25 cm^2. Before electrochemical testing, the working electrodes were activated by cyclic voltammetry of 50 sweep segments in electrolyte to generate stable active species. Linear Sweep Voltammetry (LSV) was performed in 1.0 M KOH with/without 0.5 M methanol solution. All potentials reported in this paper are with respect to reversible hydrogen electrode (RHE), which were converted by Equation 1.

Potential in RHE= Applied potential *vs* Hg/HgO + 0.098 + 0.0592pH (Equation 1).

Solar-driven electrochemical system. Unassisted solar-driven electrocatalytic reaction was achieved using a photovoltaic cell. The surface area of the photovoltaic cell was 3 cm × 3 cm, and the surface areas of the anodes and cathodes were both 1 cm^2. The device was illuminated with standard AM 1.5G solar light at room temperature, and operated at a voltage of 2.0 V (the intersection point of the current-voltage curves of the photovoltaic cell and integrated electrolysis cell). The electrochemical working station was wired in series (with 0 V applied) to monitor the current.

DFT calculations. All spin-polarized DFT calculations were carried out using the Vienna ab initio simulation package (VASP).[1,2] The Perdew-Burke-Ernzerhof (PBE) exchange-correction functional within the generalized gradient approximation (GGA) was employed to describe the exchange-correlation potential.[3,4] The DFT-D3 approach was applied to describe van der Waals (vdW) interactions.[5] A vacuum distance of 20 Å was employed to avoid interactions between periodic images. The cut-off energy of the plane wave basis was set to 450 eV. The energy and force convergence criteria were set to be 10^{-4} eV and 0.01 eV $Å^{-1}$, respectively. The Brillouin zone was sampled with a 1×1×1 by Gamma centered grids. Based on the experimental results, a three-layer slab repeated in a p(3×4) $Ni_{0.2}Mo_{0.8}N$(100) supercell with one layer of F,N-C@NF or N-C@NF at the bottom was built as $Ni_{0.2}Mo_{0.8}N$/F,N-C@NF or $Ni_{0.2}Mo_{0.8}N$/N-C@NF. A p(2×2) Ni_3N(100) supercell with one layer of F,N-C@NF or N-C@NF at the bottom was built as Ni_3N/F,N-C@NF or Ni_3N/N-C@NF. The d-band center of Mo or Ni atom was calculated by the equation, $\varepsilon_d = \frac{\int_{-\infty}^{+\infty} \rho_d(E) E \, dE}{\int_{-\infty}^{+\infty} \rho_d(E) \, dE}$, where ρ_d and E represent the projected density of states of the d orbitals of the Mo or Ni atom and the energy about the Fermi level, respectively. The adsorption energy (E_{ads}) of the adsorbed *OH_2 on the $Ni_{0.2}Mo_{0.8}N$/F,N-C@NF, $Ni_{0.2}Mo_{0.8}N$/N-C@NF, Ni_3N/F,N-C@NF or Ni_3N/N-C@NF is expressed by $E_{ads} = E_{total} - E_{H_2O} - E_{catalyst}$, in which E_{total}, E_{H_2O}, and $E_{catalyst}$denote the total energies of the adsorbed *OH_2, the isolated H_2O, and the $Ni_{0.2}Mo_{0.8}N$/F,N-C@NF, $Ni_{0.2}Mo_{0.8}N$/N-C@NF, Ni_3N/F,N-C@NF or Ni_3N/N-C@NF, respectively. The bonding/anti-bonding population between the catalysts and intermediates was analyzed using the projected crystal orbital Hamilton population (pCOHP).[6] According to the computational hydrogen electrode (CHE) model,[7] the Gibbs free energy (ΔG_{H^*}) was defined as: $\Delta G_{H^*} = \Delta E_{H^*} + \Delta ZPE -$

TΔS, where ΔE_{H^*} is the adsorption energy of H* adsorption, ΔZPE and ΔS are the differences in the zero-point energy and entropy. T is the room temperature of 298.15 K.

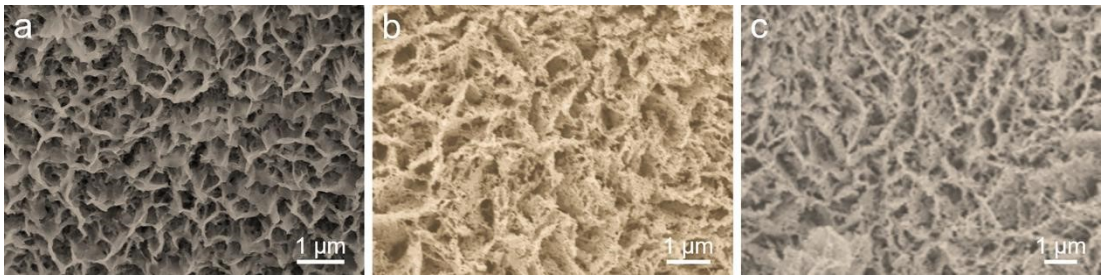

Fig. S1 SEM images of (a) $Ni_{0.2}Mo_{0.8}N$/N-C@NF, (b) Ni_3N/F,N-C@NF and (c) Ni_3N/N-C@NF.

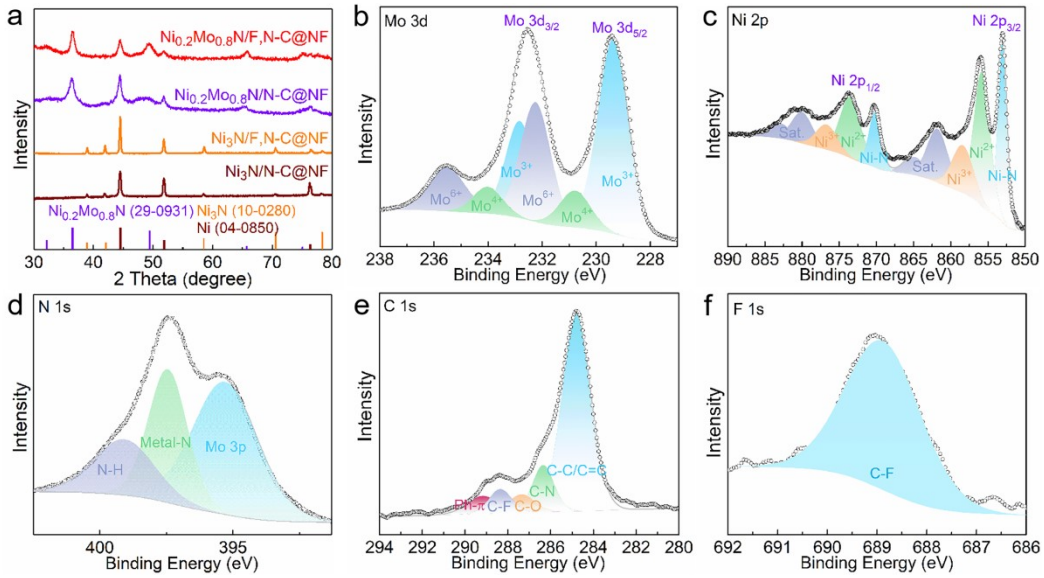

Fig. S2 (a) XRD patterns of prepared catalysts. High-resolution XPS spectra of (b) Mo 3d, (c) Ni 2p, (d) N 1s, (e) C 1s and (f) F 1s of $Ni_{0.2}Mo_{0.8}N$/F,N-C@NF.

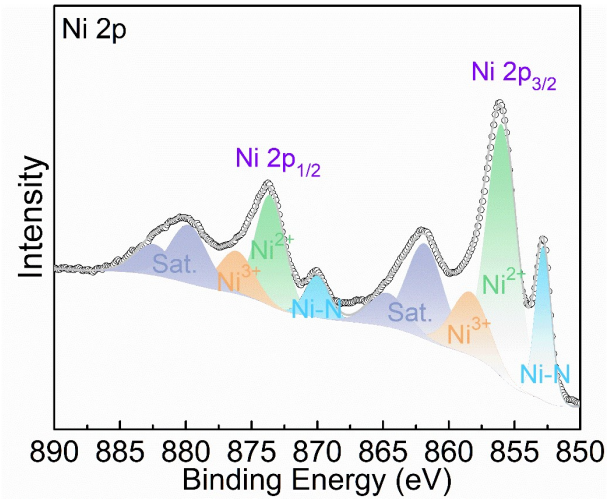

Fig. S3 High-resolution XPS spectra of Ni 2p of Ni_3N/N-C@NF.

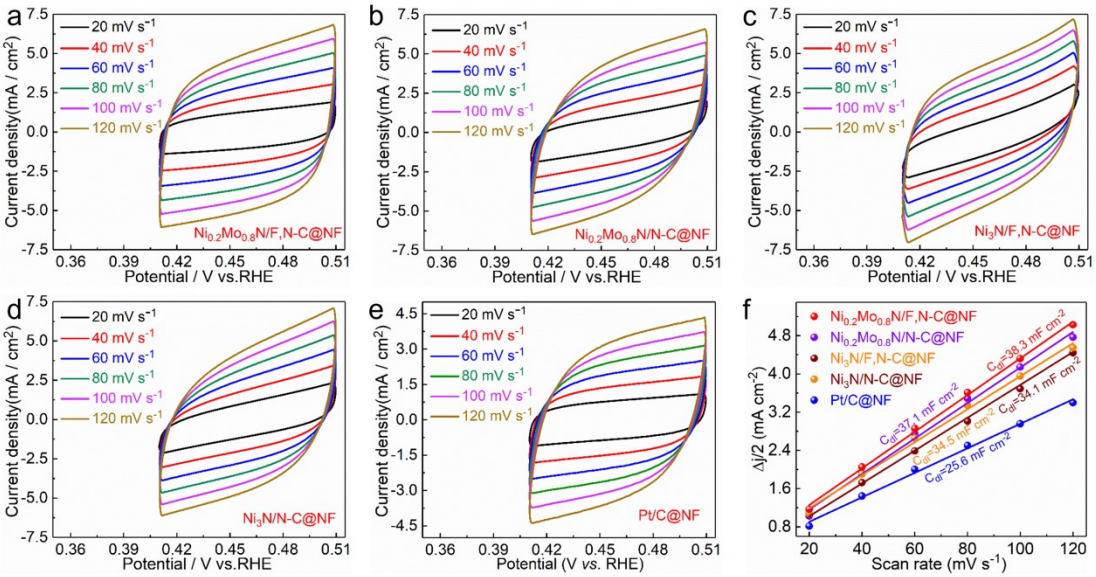

Fig. S4 CV curves acquired at various scan rates in 1.0 M KOH solution of (a) $Ni_{0.2}Mo_{0.8}N$/F,N-C@NF, (b) Ni_3N/F,N-C@NF, (c) $Ni_{0.2}Mo_{0.8}N$/N-C@NF (d) Ni_3N/N-C@NF and (e) Pt/C@NF. (f) The double-layer capacitances derived from the CV curves at various scan rates.

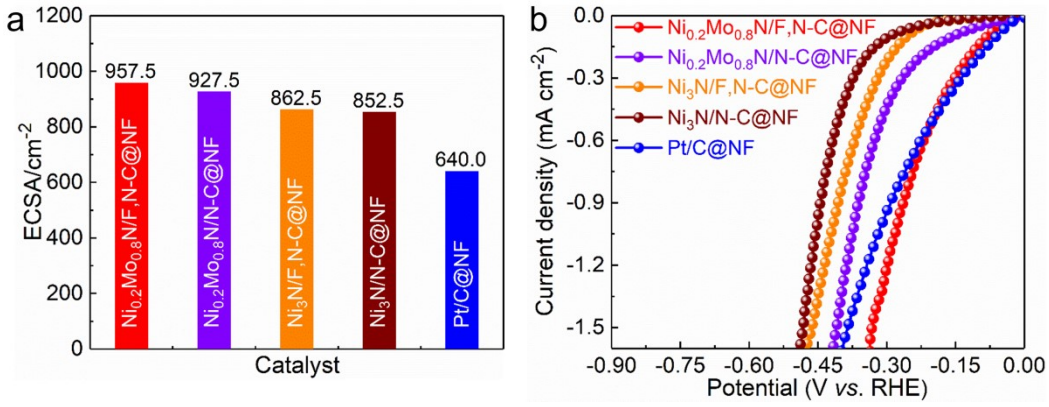

Fig. S5 (a) The electrochemical active areas of $Ni_{0.2}Mo_{0.8}N$/F,N-C@NF, $Ni_{0.2}Mo_{0.8}N$/N-C@NF, Ni_3N/F,N-C@NF, Ni_3N/N-C@NF and Pt/C@NF. (b) HER polarization curves normalized by ECSA for $Ni_{0.2}Mo_{0.8}N$/F,N-C@NF, $Ni_{0.2}Mo_{0.8}N$/N-C@NF, Ni_3N/F,N-C@NF, Ni_3N/N-C@NF and Pt/C@NF.

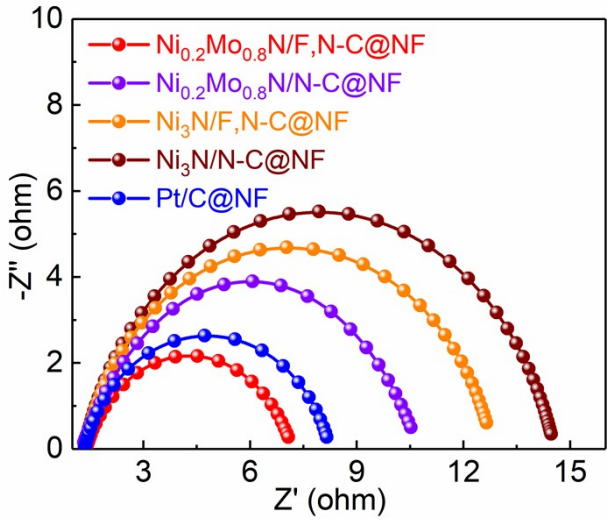

Fig. S6 Nyquist plots for $Ni_{0.2}Mo_{0.8}N$/F,N-C@NF, $Ni_{0.2}Mo_{0.8}N$/N-C@NF, Ni_3N/F,N-C@NF and Ni_3N/N-C@NF.

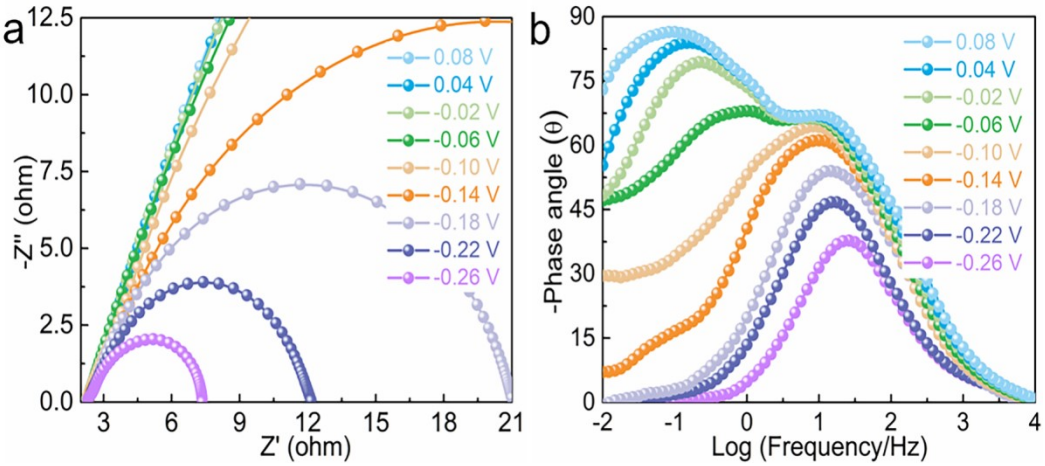

Fig. S7 (a) Nyquist and (b) Bode plots for Ni_3N/N-C@NF.

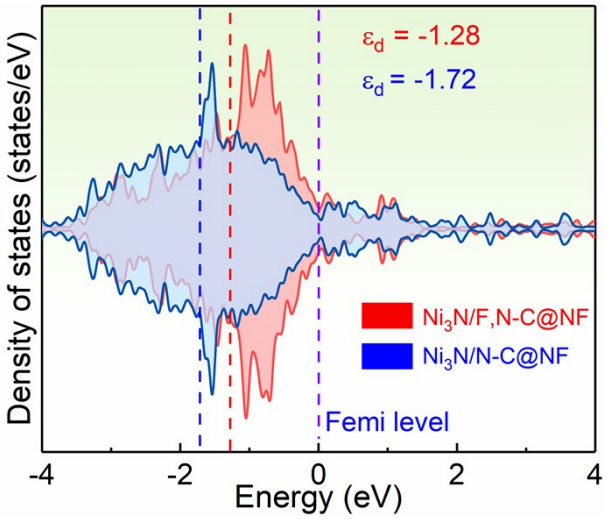

Fig. S8 Density of states (DOS) of Ni_3N/F,N-C@NF and Ni_3N/N-C@NF.

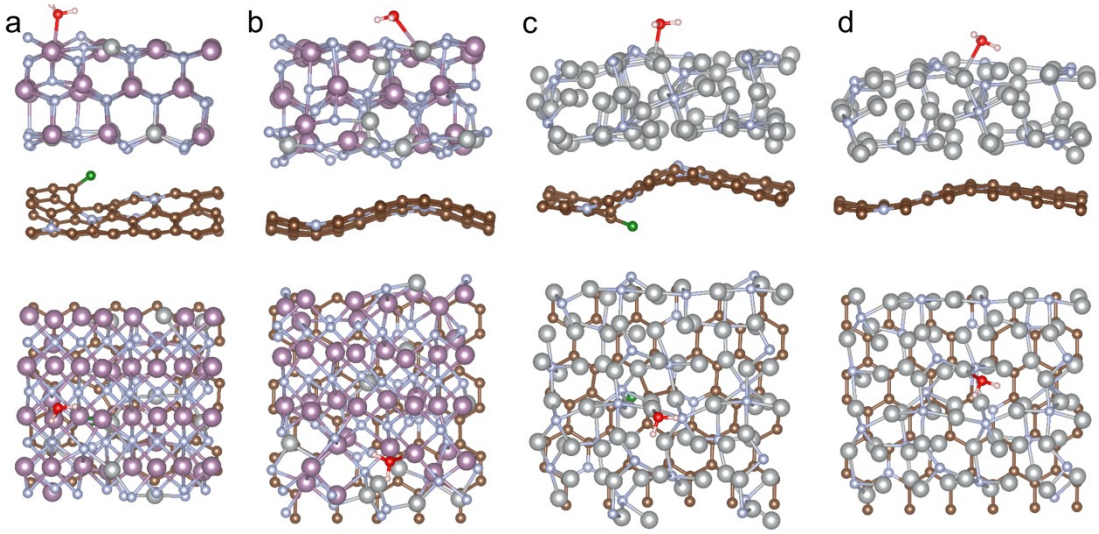

Fig. S9 The geometric configurations of the *OH_2 adsorbed on $Ni_{0.2}Mo_{0.8}N$/F,N-C@NF, $Ni_{0.2}Mo_{0.8}N$/N-C@NF, Ni_3N/F,N-C@NF and Ni_3N/N-C@NF.

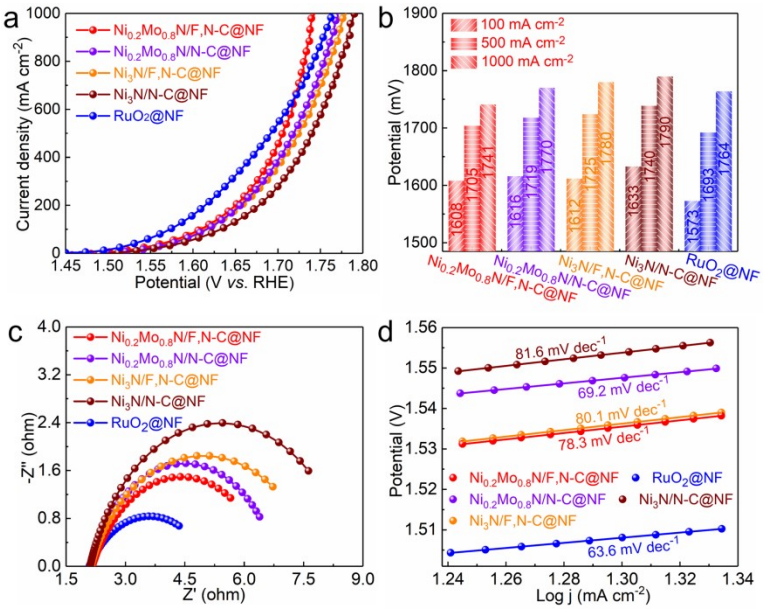

Fig. S10 (a) LSV curves of the catalysts and commercial RuO_2@NF in 1.0 M KOH solution with a scan rate of 5 mV s^{-1}. (b) Comparison of the potentials at 100, 500 and 1000 mA cm^{-2}, (c) the EIS Nyquist plots, (d) the corresponding Tafel slopes of the catalysts and commercial RuO_2@NF.

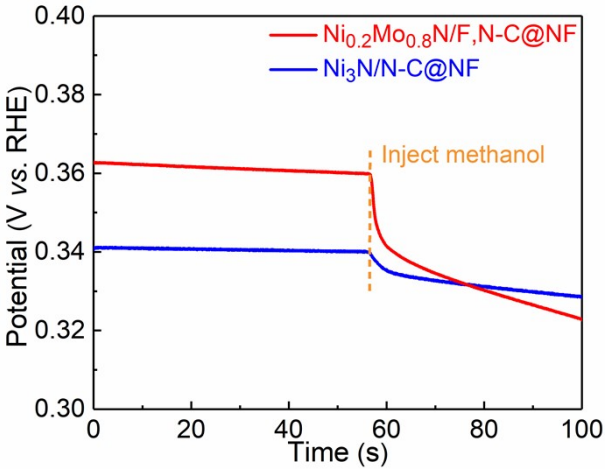

Fig. S11 The OCP of the $Ni_{0.2}Mo_{0.8}N$/F,N-C@NF and Ni_3N/N-C@NF in 1.0 M KOH solution before and after methanol was injected.

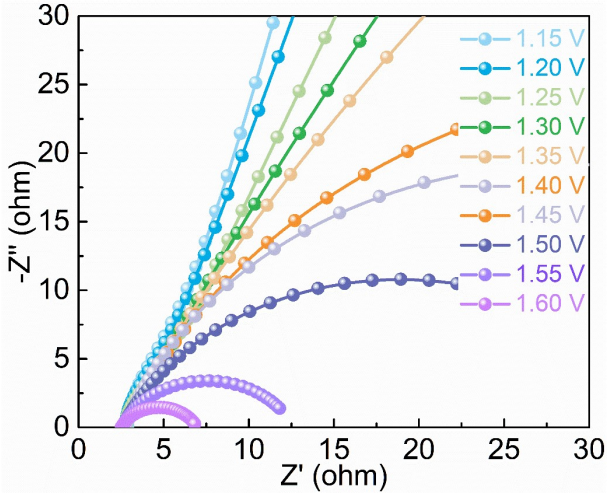

Fig. S12 The potential-dependent Nyquist of $Ni_{0.2}Mo_{0.8}N$/F,N-C@NF for OER.

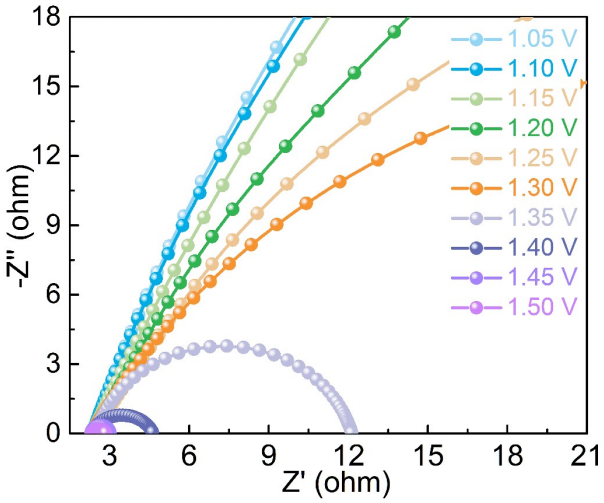

Fig. S13 The potential-dependent Nyquist of $Ni_{0.2}Mo_{0.8}N$/F,N-C@NF for MOR.

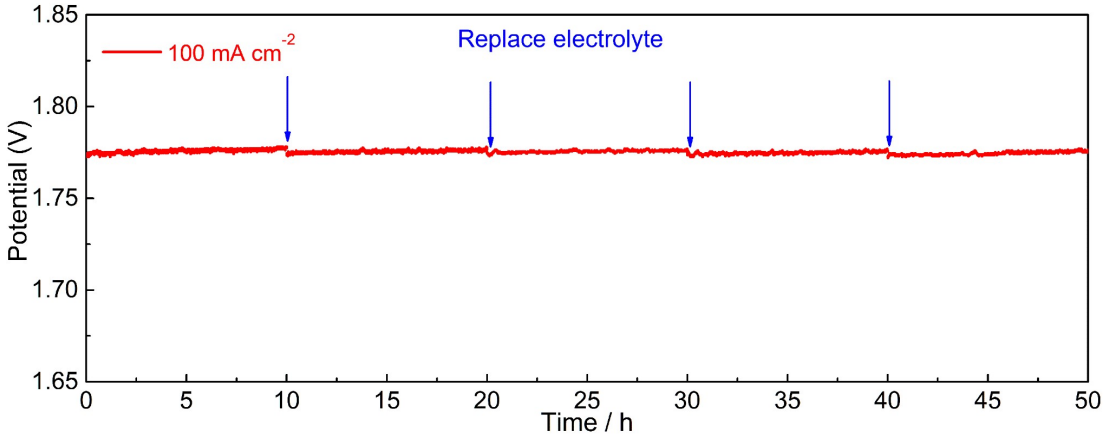

Fig. S14 The chronopotentiometry curve of the $Ni_{0.2}Mo_{0.8}N/F,N\text{-}C@NF$ under a current density of 100 mA cm^{-2}.

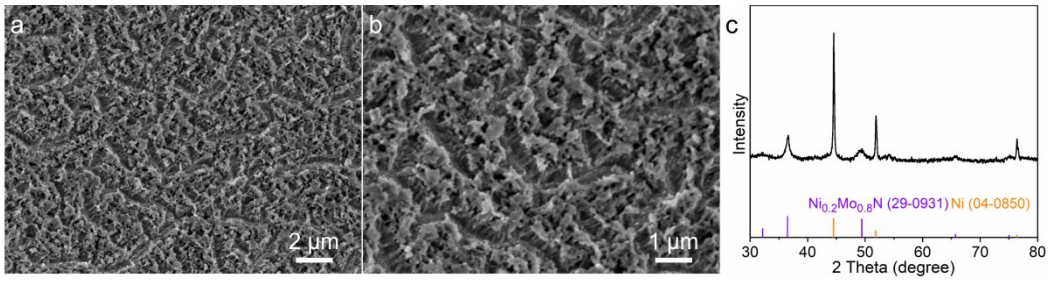

Fig. S15 (a, b) SEM images and (c) XRD pattern of $Ni_{0.2}Mo_{0.8}N$/F,N-C@NF after stability testing.

Table S1 Comparison of the HER activity of $Ni_{0.2}Mo_{0.8}N$/F,N-C@NF with other published electrocatalysts.

Catalyst	Current density (mA cm^{-2})	Overpotential (mV)	Reference
$Ni_{0.2}Mo_{0.8}N$/F,N-C@NF	100	83	This work
	500	204	
	1000	281	
MnO-CoP/NF	100	94.5	8
	500	186.2	
	1000	259.5	
Cu-FeOOH/Fe_3O_4	100	129	9
	500	285	
	1000	349	
Ni_3S_2/Cr_2S_3@NF	100	160	10
	500	207	
	1000	267	
NMFSOH	100	128	11
	500	175	
	1000	200	
$Ni_{0.96}Co_{0.04}P$/NF	500	161	12
	1000	251	
Ni@NCW-2.0	100	239	13
	500	385	
Ni_2P−NiMoOx/NF	100	188	14
	500	297	
Ru-Mo_2C@CNT	100	90	15
Ni_3N-C@NFo_3N	100	120	16
$Ni(OH)_2$@Ni-N/Ni-C	100	113	17
PtSA-NiSe-V	100	109	18
NiCoP	100	148	19
CoMnP-NPC/CC	100	114	20
Cr-Ni_3N	100	158	21
NiFeV@FeO_x/IF	100	105	22
NF/O-CoP	100	122.4	23
Co/CoMoN/NF	100	173	24
Ni_2P-CoCH/CFP	100	143	25
$FeWO_4$-Ni_3S_2/NF	1000	343	26

References

1 G. Kresse and J. Furthmüller, *Phys. Rev. B*, 1996, **54**, 11169−11186.

2 G. Kresse and J. Hafner, *Phys. Rev. B*, 1993, **47**, 558−561.

3 J. Perdew, K. Burke and M. Ernzerhof, *Phys. Rev. Lett.*, 1996, **77**, 3865−3868.

4 P. Blöchl, *Phys. Rev. B*, 1994, **50**, 17953−17979.

5 S. Grimme, J. Antony, S. Ehrlich and H. Krieg, *J. Chem. Phys.*, 2010, **132**, 154104.

6 S. Maintz, V. Deringer, A. Tchougréeff and R. Dronskowski, *J. Comput. Chem.*, 2016, **37**, 1030−1035.

7 J. Nørskov, J. Rossmeisl, A. Logadottir, L. Lindqvist, J. Kitchin, T. Bligaard and H. Jónsson, *J. Phys. Chem. B*, 2004, **108**, 17886−17892.

8 Y. Dong, Z. Deng, H. Zhang, G. Liu and X. Wang, *Nano Lett.*, 2023, **23**, 9087−9095.

9 C. Yang, W. Zhong, K. Shen, Q. Zhang, R. Zhao, H. Xiang, J. Wu, X. Li and N. Yang, *Adv. Energy Mater.*, 2022, **12**, 2200077.

10 H. Q. Fu, M. Zhou, P. F. Liu, P. Liu, H. Yin, K. Z. Sun, H. G. Yang, M. Al-Mamun, P. Hu, H.-F. Wang and H. Zhao, *J. Am. Chem. Soc.*, 2022, **144**, 6028−6039.

11 P. Fang, M. Zhu, J. Liu, Z. Zhu, J. Hu and X. Xu, *Adv. Energy Mater.*, 2023, **13**, 2301222.

12 X. Lv, S. Wan, T. Mou, X. Han, Y. Zhang, Z. Wang and X. Tao, *Adv. Funct. Mater.*, 2023, **33**, 2205161.

13 D. Li, H. Cheng, X. Hao, G. Yu, C. Qiu, Y. Xiao, H. Huang, Y. Lu and B. Zhang, *Adv. Mater.*, 2023, **36**, 2304917.

14 J. Ren, L. Chen, H. Wang, W. Tian, X. Song, Q. Kong and Z. Yuan, *ACS Catal.*, 2023, **13**, 9792−9805.

15 X. Wu, Z. Wang, D. Zhang, Y. Qin, M. Wang, Y. Han, T. Zhan, B. Yang, S. Li, J. Lai and L. Wang, *Nat. Commun.* , 2021, **12**, 4018.

16 Q. Qian, J. Zhang, J. Li, Y. Li, X. Jin, Y. Zhu, Y. Liu, Z. Li, A. El-Harairy, C. Xiao, G. Zhang and Y. Xie, *Angew. Chem., Int. Ed.*, 2021, **60**, 5984−5993.

17 K. Dastafkan, X. Shen, R. K. Hocking, Q. Meyer and C. Zhao, *Nat. Commun.* , 2023, **14**, 547.

18 Z. Chen, X. Li, J. Zhao, S. Zhang, J. Wang, H. Zhang, J. Zhang, Q. Dong, W. Zhang, W. Hu and X. Han, *Angew. Chem., Int. Ed.*, 2023, **62**, e202308686.

19 G. Ma, J. Ye, M. Qin, T. Sun, W. Tan, Z. Fan, L. Huang and X. Xin, *Nano Energy*, 2023, **115**, 108679.

20 Y. Xu, S. Wei, L. Gan, L. Zhang, F. Wang, Q. Wu, X. Cui and W. Zheng, *Adv. Funct. Mater.*, 2022, **32**, 2112623.

21 S. Li, S. Wang, J. He, K. Li, Y. Xu, M. Wang, S. Zhao, Y. Wang, X. Li, X. Zhong and J. Wang, *Angew. Chem., Int. Ed.*, 2023, **62**, e202306553.

22 H. Yao, F. Le, W. Jia, Y. Cao, R. Sheng, Z. Lu, X. Chen and D. Jia, *Small*, 2023, **19**, 2301294.

23 Y. Dong, Z. Deng, Z. Xu, G. Liu and X. Wang, *Small Methods*, 2023, **7**, 2300071.

24 H. Ma, Z. Chen, Z. Wang, C. V. Singh and Q. Jiang, *Adv. Sci.*, 2022, **9**, 2105313.

25 S. Zhang, C. Tan, R. Yan, X. Zou, F. Hu, Y. Mi, C. Yan and S. Zhao, *Angew. Chem., Int. Ed.*, 2023, **62**, e202302795.

26 Z. Wang, G. Qian, T. Yu, J. Chen, F. Shen, L. Luo, Y. Zou and S. Yin, *Chem. Eng. J.*, 2022, **434**, 134669.